Research Article

Nawal M. Al Musayeib, Musarat Amina*, Hanan M. Al-Yousef, Mohsin ul Haq, Sooad Al-Daihan, and Ramesa Shafi Bhat*

Rhus microphylla-mediated biosynthesis of copper oxide nanoparticles for enhanced antibacterial and antibiofilm efficacy

https://doi.org/10.1515/gps-2024-0102
received May 06, 2024; accepted October 8, 2024

Abstract: The global emergence and tenacity of multidrug-resistant microbes have raised new challenges for the management of diseases associated with infections. Metal-based nanoparticles (NPs) have recently received special attention as a prospective alternate for existing chemical antibiotics because of their extensive antibacterial potency and low toxicity. Herein, copper nanoparticles (CuONPs) were prepared by using an aqueous extract of aerial parts *Rhus microphylla* (RM) aerial parts. The obtained RM-CuONPs were characterized and evaluated for antimicrobial and antibiofilm potential against various human pathogens. The formed RM-CuONPs were well dispersed with a uniform spherical shape and an average size of 32.45 nm. Numerous functional moieties found in the FTIR spectra confirmed that the phytocomponents of the RM-extract were in charge of the synthesis synthesis, capping, and stabilization of RM-CuONPs. The biogenic RM-CuONPs demonstrated superior antibacterial effectiveness towards *Staphylococcus epidermidis* and *Enterobacter cloacae* with a minimum inhibitory concentration (MIC) value of 48.5 μg·mL^{-1}. Remarkable antifungal activity of RM-CuONPs was noted against *C. tropicalis* (MIC = 97 μg·mL^{-1}). Also, the biosynthesized RM-CuONPs demonstrated notable potential in reducing biofilm formation in a dose-dependent manner. These inferences offer an insight into the plausible for utilizing plant extracts for the biosynthesis of CuONPs with enhanced biological activity and could offer promising effective substitutes to traditional antimicrobials for the treatment of biofilms and drug-resistant bacteria.

Keywords: copper oxide nanoparticles, biosynthesis, antibacterial, antibiofilm, *Rhus microphylla*

1 Introduction

Nanomaterials have garnered more attention in recent times because of their prominent application in various domains, including materials science, medicine, biotechnology, and energetics [1]. Due to their size, distribution, and morphology, these nano-sized materials have novel and enhanced beneficial features which differentiate them from their counterpart bulk material [2]. As nanomaterials continue to be developed metal oxide nanoparticles (NPs) exhibit plenty of fascinating prospects in the biomedical field, particularly in the areas of antimicrobial and anticancer therapies, drug delivery, biosensing, and cell imaging [3]. Among these materials, copper oxide (CuO) NPs are considered a versatile candidate for biocompatible applications due to their biocompatibility, cost benefit, and low toxicity [4]. Their notable optical, structural, and biological properties, large surface area, chemical stability, enhanced stability-to-weight ratio, superior characteristics, and reusable nature render them suitable materials for industrial as well as biomedical applications [5]. Several conventional approaches, including biological, hydrothermal, solvothermal, and thermolysis of a few source precursor components, have been used to synthesize CuONPs [6]. All the physical procedures require high temperature and pressure, which rather are pretty pricey [7]. On the other hand, the use of

* **Corresponding author: Musarat Amina,** Department of Pharmacognosy, College of Pharmacy, King Saud University, Riyadh, 11495, P.O. Box 22452, Saudi Arabia, e-mail: mamina@ksu.edu.sa
* **Corresponding author: Ramesa Shafi Bhat,** Department of Biochemistry, College of Science, King Saud University, Riyadh, 11451, Saudi Arabia, e-mail: rbhat@ksu.edu.sa
Nawal M. Al Musayeib: Department of Pharmacognosy, College of Pharmacy, King Saud University, Riyadh, 11495, P.O. Box 22452, Saudi Arabia, e-mail: nalmusayeib@ksu.edu.sa
Hanan M. Al-Yousef: Department of Pharmacognosy, College of Pharmacy, King Saud University, Riyadh, 11495, P.O. Box 22452, Saudi Arabia, e-mail: halyousef@ksu.edu.sa
Mohsin ul Haq: Department of Pharmacognosy, College of Pharmacy, King Saud University, Riyadh, 11495, P.O. Box 22452, Saudi Arabia, e-mail: mohsin.ibnhaq@yahoo.com
Sooad Al-Daihan: Department of Biochemistry, College of Science, King Saud University, Riyadh, 11451, Saudi Arabia, e-mail: sdaihan@ksu.edu.sa

chemical materials as reducers in chemical procedures has a negative effect on the environment and users, leading to several problems [8]. In contrast to these prior approaches, the green synthesis approach has lately introduced a facile and ecologically conscious route to synthesize them [9]. Biological resources, including; plant extracts, plants, bacteria, fungi, enzymes, and marine organisms are used in this process to create nanomaterials, and have several benefits for biomedical applications [10]. Out of all the natural resources, plants are favored over the others for the production of nanomaterials due to the presence of an array of phytochemicals, including flavonoids, glycosides, polyphenols, terpenoids, and enzymes, that function as reducing and capping agents for the synthesis of nanostructures with desired shape and size [11]. Plants are also preferred on competing biological techniques as they preclude the need for lengthy culturing times of microorganism as well as preservation [12]. Notably, plant extracts, inheriting therapeutic properties, can be utilized to obtain NPs with enhanced biological potential [13]. The current work exploits green methodology for the synthesis of CuONPs using a crude aqueous extract of *R. microphylla* (RM) and its anatomical components.

RM Engelm. ex A. Gray is a wild plant and a member of the family *Anacardiaceae* found in Central America, Mexico, and Southwestern United States [14]. It is a perennial shrub with branches that may grow up to 3 m tall. It has red fruits, glandular trichomes, and simple, evergreen leaves. The fruits of RM have locally been consumed as beverages and condiments by Kickapoo, the indigenous people of United States of America and Mexico [15]. The plant contains a plethora of phytoconstituents, including phenolic acids, flavonoids, betacyanins, betaxanthins, carbohydrates, and vitamins [16,17]. The fruits of this plant are a rich source of gallic acid, *p*-coumaric acid, +epicatechin, and ellagic acid [17]. Different extracts of RM have been reported for their antioxidant, antibacterial, and fungal activities [18].

Nanomaterials have been utilized extensively in medical applications due to their noteworthy and unique traits, such as quantum size effect, notably larger surface to mass ratio, adsorption capacity and ability to transfer materials like proteins, drugs, and probes, when compared to other particles [19].

Extensive research on antimicrobial resistance has demonstrated that pathogen that are resistant to antibiotics reside in biofilms, rather than as free bacteria [20]. Traditional antimicrobials are resistant to bacteria forming biofilm because (1) the inability of the antimicrobial to enter the biofilm, (2) development of intricate medication features and (3) alteration of antimicrobial enzymes by biofilms [21]. Interestingly, NP-based antimicrobials have been introduced and marketed to obliterate bacteria that are resistant to antibiotics and can form both planktonic and biofilm formation. Numerous studies have addressed the antibacterial potential of elemental Cu, CuO, and Cu_2O, relating their morphology, particle size effect, and copper ion dissolution in different media [22–24]. Copper exhibits effective microbial inhibition by inflicting impairment to various functions of cells and exerting cytotoxicity [25]. The mechanism involves the generation of reactive oxygen species (ROS) and the replacement or native cofactors binding in metalloproteins. Additionally, copper plays a key role in intrinsic immunity, catalyzing ROS formation during phagocytosis and enhancing bactericidal activity [26]. The CuONPs employ similar mechanisms as displayed by other copper materials, with studies suggesting that metallic NPs possess stronger antimicrobial properties than their larger counterparts [27,28]. This heightened effectiveness is given credit for having a bigger surface area and unique crystal structure of CuONPs, influencing various cellular components in microbial cells through distinctive mechanisms [29,30]. The faster dissolution of CuONPs in solutions makes more metal ions available for release resulting in a more potent antimicrobial effect [31]. Furthermore, they are capable of concurrently activating diverse antibacterial pathways making it difficult for microorganisms acquire several gene alterations to resist these distinct antimicrobial actions [32]. Consequently, the likelihood of antimicrobial resistance is low. Biofilms represent intricate communities of microorganisms that exhibit resistance to antibiotics and the human immunological system, owing to their resilient and stable nature [33]. Eradicating biofilm infections poses a significant challenge, particularly in cases involving multidrug-resistant pathogens [34,35]. Both Gram-positive and Gram-negative bacteria are capable of forming biofilms and diseases linked to these biofilms are distinguished by persistent infections with slow development, showcasing the ability to withstand the immunological system of host and momentary reaction to antibiotic therapy [36]. Biofilms formed by some fungal strains of *Candida* inherently display resistance to traditional antifungal treatments as well as challenges from the host immune system, which pose a substantial clinical hurdle in managing infections [37]. Numerous reports have detailed the versatile potential of CuONPs as effective antimicrobial agents [38].

Owing to the massive significance of green and sustainable plant-mediated metal/metal oxide NP synthesis and promising antimicrobial profile of CuONPs, the aim of the current study was to utilize the copper ion reduction in synthesizing nano-sized materials using the RM plant extract. The present work described a facile, economical, environmentally benign, and green synthesis route of RM-CuONPs using readily accessible RM plants in Saudi Arabia. The aqueous extract of RM aerial parts enriched in

phenolics and flavonoids served as reducers and stabilizers for the prospective utilization of the biogenic RM-CuONPs as antimicrobial agents. The novelty aspect of this study is that for the first time RM aerial parts were utilized for the formation of RM-CuONPs. The formed NPs were properly characterized by advanced analytical and microscopic techniques. In addition, the biosynthesized RM-CuONPs were explored for their antimicrobial and anti-biofilm activity against a panel of human pathogens. The prepared RM-CuONPs were also tested for their antioxidant potential by the 1,1-diphenyl-2-picryl-hydrazyl (DPPH) assay. The novel pre-synthesized RM-CuONPs can serve as an intriguing antimicrobial contender with promise for application in biomedicine.

2 Materials and methods

2.1 Chemicals

Copper(II) sulfate pentahydrate ($CuSO_4{\cdot}5H_2O$, ≥98%), Mueller Hinton broth (MHB), dextrose agar, phosphate-buffered saline, and DPPH were used.

2.2 Biomass collection and preparation of extract

The aerial part of RM was obtained from rocky habitats of Madinah, Saudi Arabia, in April 2019. The collected botanical sample was recognized by a taxonomist Dr. M. Youseef, Pharmacognosy Department, King Saud University. The departmental herbarium now has a voucher specimen (RM-792) on file. The aerial parts of RM were washed with sterile distilled water to remove dust particles and then dried in the shade. The chopped dried plant material was mechanically processed into coarse powder with the help of a domestic blender. To prepare the extract of RM aerial parts, 10 g of powdered material was soaked in 500 mL of deionized water in a 500 mL beaker. After 1 h boiling, the mixture acquired the brown color in the colorless aqueous solution. The mixture was boiled for 1 h until the colorless aqueous solution changed to a brown color. The mixture was cooled, centrifuged for 5 min at 10,000 rmp and finally filtered over Whatman filter paper No.1 at room temperature to remove the biomaterials. The extraction process was conducted two more times under similar conditions. Finally, the obtained crude extract was stored was taken in air-tight glass bottles and kept cold (4°C) in fridge until needed.

2.3 Green synthesis of CuONPs

The biogenic CuONPs were synthesized by reducing copper sulfate with an aqueous extract of RM. Copper sulfate pentahydrate ($CuSO_4{\cdot}5H_2O$) was utilized as the precursor for the synthesis of CuONPs. Briefly, 150 mL of copper sulfate ($CuSO_4{\cdot}5H_2O$, 0.1 mM) was prepared in a 250 mL conical flask and then mixed with 25 mL of freshly prepared aqueous extract of RM aerial part under constant magnetic stirring at 60°C for 3 h. The change of light blue color of copper sulfate solution to a yellow color indicates the formation of copper hydroxide. The reaction mixture was then subjected to heating at 60°C under vigorous stirring until a color transition from dark yellow to dark brown was noticed, suggesting the formation of CuONPs. The fully reduced reaction mixture was centrifuged (5,000 rpm, 15 min) at ambient temperature, and the reaction mixture was collected after discarding the supernatant. The collected RM-CuONPs were oven dried at 80°C for 2 h, and after drying formed NPs were repeatedly rinsed with deionized water to free from all the impurities that were present. The dark brown RM-CuONP powder was obtained after overnight drying in an oven at 100°C and was ready for further characterization [39]. Figure 1 depicts the procedure of synthesizing CuONPs using an aqueous extract of aerial parts of RM extract and copper sulfate pentahydrate as a precursor.

The mechanism and the bioactive components responsible for the formation of NPs via plant extracts have not been entirely addressed yet [40]. The plausible mechanism of RM-CuONP formation, using the RM extract is outlined as follows:

$$nCu^{2+} \rightarrow +2Ar{-}(OH)_n \rightarrow nCu^0 + 2nAr = O + 2nH^+ \quad (1)$$

$$2(x + 1)Cu^0 + 2Ar = O + yO_2 \rightarrow 2(Cu^0{-}Cu_xO_y{-}Ar = O) \quad (2)$$

The bioactive components such as phenolic and tannins ($Ar{-}(OH)_n$) of RM extract, responsible for the formation of CuONPs, could liberate their electrons for the efficient reduction of Cu^{2+} ions into Cu^0. This might result in the formation of a Cu^0–phenolate complex by the chelating effect causing the growth and nucleation of NPs at 60°C. The formed complex undergoes decomposition at a higher temperature (100°C) in air and leads to the generation of RM-CuONPs. Thus, the natural phenolics present in the RM extract had favorable effects on the biosynthesis of RM-CuONPs.

2.4 Characterization

The biosynthesized RM-CuONPs were characterized by measuring their absorption spectra in the 200–800 nm

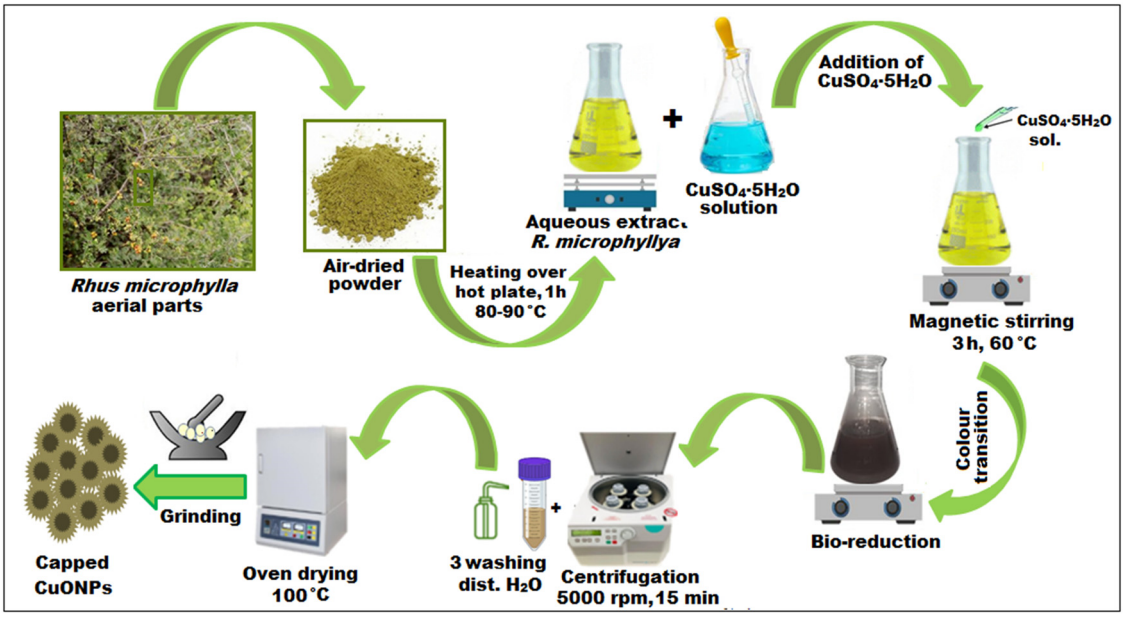

Figure 1: Schematic representation of RM-CuONPs using an aqueous extract of RM aerial parts as a reducing agent and copper sulfate as a precursor.

range on a double-beam UV–vis spectrophotometer (UV-2450, Shimadzu). Fourier transform infrared (FT-IR) analysis using KBr pellets in the 4,000–400 cm^{-1} range was implemented to identify the functional moieties involved in the precursor reduction into NPs (8400S spectrometer, Shimadzu). X-ray diffraction (XRD; 6000-XRD, Shimadzu) was performed at a scanning rate of 20°C·min^{-1} with 2θ in the 20°–80° range to obtain the structural information, crystallite size, and lattice constant of RM-CuONPs. The surface morphology of the formed RM-CuONPs was observed under scanning electron microscopy (SEM, JEOL JSM-6480, LV). A JEOL-2010 microscope running at 200 kV accelerating voltage was employed to record transmission electron micrographs (TEM). Energy-dispersive X-ray spectroscopy (EDS/EDX) coupled with SEM was applied to explore the atomic-level composition of the formed NPs. Zeta potential results were performed on a zeta potential/particle size analyzer (Brookhaven).

2.5 Antimicrobial and anti-biofilm activity

2.5.1 Microbial strains

The 13 clinical isolates used in this study were Gram-positive strains of *Staphylococcus epidermidis, Enterococcus faecalis, Staphylococcus aureus, Streptococcus pneumoniae*, and *Bacillus subtilis*; Gram-negative strains of *Escherichia coli, Enterobacter cloacae, Klebsiella pneumoniae, Pseudomonas aeruginosa, Providencia stuartii,* and *Salmonella typhi*; whereas, two fungal strains used were C*andida albicans* and *Candida tropicalis*. King Khalid Hospital in Riyadh provided all test strains. Before usage, all bacterial strains were reactivated on Mueller-Hinton agar (MHA) plates, and all fungal strains were reinstated on dextrose agar (SDA) plates respectively.

2.5.2 Antibacterial activity

The antibacterial effect was assessed by employing the well diffusion test. Every strain of bacteria had their overnight broth cultures adjusted to approximately 10^6 CFU·mL^{-1}. About 20 µL was dispersed using a sterile cotton swab over 20 mL of sterilized agar plates. For around 3 min, the medium's surface was allowed to dry. Sterile wells of 6 mm diameter were placed into the plates, and 100 L of test sample was put into every well to conduct the experiment. Following an incubation period of 24 h at 37°C, the diameter of the inhibitory zone (measured in mm) was applied to quantify the extent of microbial growth. Each test sample underwent three inspections, and the mean results are presented.

2.5.3 Determination of minimum inhibitory concentration (MIC)

MIC was determined by the broth micro-dilution procedure. In 96-well microtiter plates, the test solutions were serially diluted twice in MHB to reach the desired final concentrations ranging from 0. About 195–100 mg·mL^{-1}

for the plant extract and from 0.097 to 50 mg·mL^{-1} for NPs. Then, each well was added with 100 mL of log-phase microbial culture adjusted to around 10^6 CFU·mL^{-1}. The turbidity of media was observed for the bacterial growth after being incubated at 37°C for 16–18 hrs. The MIC was taken as the lowest concentration of extract or antibiotics necessary to limit microorganism growth without medium becoming turbid. Each assay was carried out three times.

2.5.4 Determination of minimum bactericidal concentration (MBC)

The test solutions in wells showing bacterial inhibition in the broth microdilution procedure mentioned above were laid on MHA and those showing fungal inhibitions were plated on dextrose agar and incubated at 37°C for 16–18 h. The MBC was taken as the most minimal extract or NPs concentration that was able to eradicate 99.9% of bacteria or fungi, displaying no growth on plates. Three duplicates of each assay were performed.

2.5.5 Determination of biofilm formation by the microtiter plate method

The influence of the extract and synthesized NPs on the biofilm establishment of the three most sensitive strains was tested through the microdilution method. Each microbial strain was nurtured in MHA for an entire night. After culture was diluted to 10^6 CFU·mL^{-1} it was put onto a 96-well microtiter plate containing two-fold serial dilutions of extract and NPs at 4MIC, 2MIC, MIC, 1/2MIC, and 1/4MIC. The control wells contained bacterial strains without extract and NPs, and there was just MHA in negative control wells. After incubation at 37° for 3 days, cells were dumped out by turning the plate over every well was rinsed with 200 µL of sterilized phosphate-buffered saline. Each well received 125 µL of 0.1% solution of crystal violet and incubated at ambient temperature for 15 min. Excess stains were rinsed away under running tap water. After letting the plates for air drying, 120 µL of glacial acetic acid (30%, v/v) was used to solubilize the stained biofilms. The amount of biofilm formed was quantified by measuring optical density (OD) at 570 nm, using an automatic micro ELISA plate. In qualitative assays, the wells were photographed.

2.6 Antioxidant activity

The ability of biosynthesized RM-CuONPs, aqueous RM extract, and standard L-ascorbic acid to scavenge the free radicals of DPPH at varied concentrations (5–140 µg·mL^{-1}) was conducted by following the method of Schlesier et al. [41]. In brief, 2 mL of DPPH solution was poured into 0.1 mL of varying concentrations of each test sample and standard ascorbic acid and mixed well. After vigorous shaking for 1 min, the reaction mixture was given dark exposure for 30 min at ambient temperature and at 517 nm wavelength absorbance was noted with a UV-double beam spectrophotometer (UV-2900, Hitachi, Tokyo, Japan). Each assessment was performed in triplicate. The inhibition percentage of free radical (DPPH) was employed to indicate the capacity of each test sample to scavenge free radicals and was determined by applying the following equation:

$$\text{Inhibition (\%)} = \frac{A_C - A_S}{A_C} \times 100$$

where sample and control absorbance was represented by A_c and A_s, respectively. The doses of the corresponding sample curve and the free radical scavenging ability relationship curve was used to obtain the IC_{50} values.

2.7 Statistical analysis

The results of antimicrobial activities were provided as the mean ± standard deviation (SD), and there were three replicates of each experiment.

3 Results and discussion

3.1 Synthesis and characterization of CuONPs

The green/biological synthesis approaches are currently far more effective than an array of physico-chemical procedures. The main reason for the effectiveness of these green/biological approaches lies in their ability to manipulate biological entities, including plants, fungi, bacteria, and algae, without the use of pricey hazardous chemicals and high energy intake [42]. The findings represented here utilize the extract of RM aerial parts as agents for surface capping, stabilization, and reduction in the biosynthesis of RM-CuONPs. The green synthesis of RM-CuONPs was assessed by the swift color change from yellowish to brown on account of the interaction between the precursor salt ($CuSO_4{\cdot}5H_2O$) and the reducing agent under constant stirring. The UV–vis spectral estimation was conducted mainly to confirm the formation of biogenic RE-CuONPs. Figure 2a displays the spectra of RM extract and biogenic RM-CuONPs

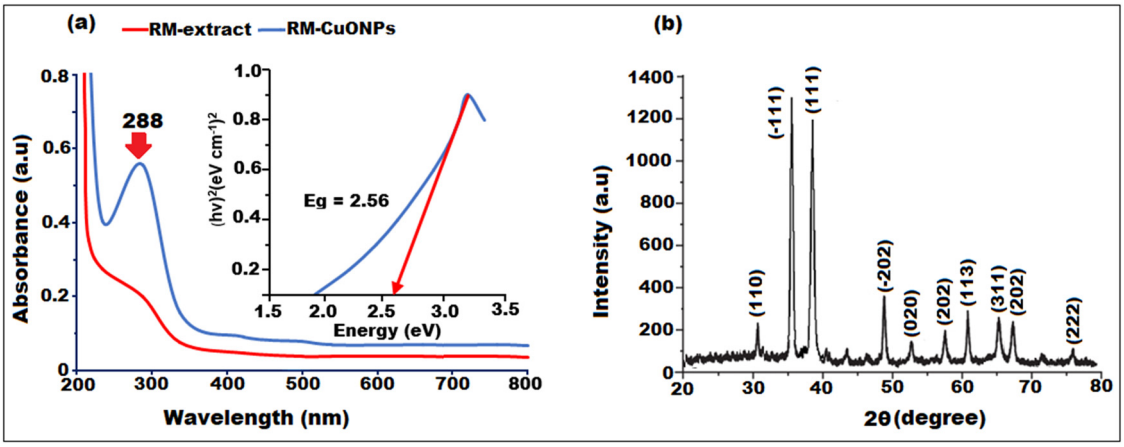

Figure 2: (a) UV–vis spectrum and bandgap energy (inset) of biosynthesized RM-CuONPs. (b) XRD pattern of biosynthesized RM-CuONPs.

after UV–vis spectroscopic analysis in the 200 to 700 nm range. The UV–vis absorption spectrum of pre-synthesized RM-CuONPs demonstrated a pronounced absorption peak at 288 nm (Figure 2a), which is specific to CuONPs [43]. The surface plasmon resonance (SPR) of RM-CuONPs is responsible for this peak, and a broad SPR peak clearly demonstrates the polydispersity of the RM-CuONPs. These findings assure that phenolic and flavonoid contents in the RM extract successfully reduced the CuO precursor to form RM-CuONPs. The bandgap energy of the formed RE-CuONPs was measured by expanding the linear component graph and plotting energy (E_g) versus $(\alpha hv)^2$, as illustrated in Figure 2a. The bandgap value of RE-CuONPs was calculated by applying the Tauc equation: $\alpha(hv)^2 = A(hv - E_g)$, where α, h, v, A, and E_g are the absorption coefficient, Planck's constant, frequency, proportionality constant, and bandgap energy, respectively. The value of bandgap energy computed for RE-CuONPs was found to be 2.56, which coincides with the earlier documented energy bandgap estimations for CuO NPs [44]. A notable decrease in the bandgap energy could be attributed to bioactive components of the plants, which modify the surface and decrease the bandgap of formed NPs. Generally, green synthesized NPs are often more reactive than their conventionally produced counterparts [44].

The rapid synthesis of RM-CuONPs was strongly confirmed by XRD, and the X-ray diffractogram was used to estimate the particle size and various crystalline aspects of pre-synthesized RM-CuONPs. The XRD spectrum of biogenic RM-CuONPs revealed the existence of sharp distinct peaks at 2θ values of 32.30°, 35.42°, 38.92°, 48.65°, 57.13°, 61.59°, 66.41°, 68.23°, and 75.65° corresponding to (110), (−111), (111), (−202), (202), (113), (311), (202), and (222) lattice planes, respectively (Figure 2b). The resultant XRD pattern matched well with the JCPDS file no. 01-080-0076, indicating that the NPs were formed with a densely packed, monoclinic structure, which confirmed the crystalline nature and small crystallite size of the formed RM-CuONPs [45]. The formed RM-CuONPs were found to be in a monoclinic phase, as evidenced by the prominent peak in the (−111) direction. These results demonstrate that the crystalline form of CuONPs produced comparable types of peak indices as reported in the investigation that was conducted by Taghavi et al. [46].

The average crystallite sizes of the biogenic RM-CuONPs were obtained from XRD data in Figure 1b, using Debye–Scherrer's formula. The computed values of crystallite size are listed in Table 1.

The computed average crystallite size of pre-synthesized RM-CuONPs was 42.43 nm. The decrease in average crystallite size of RM-CuONPs was due to the influence of phyto-constituents that develop, control, and stabilize the formed crystals. However, the strain (ε) created in the NPs as a result of crystal distortion and imperfection was

Table 1: Particle sizes of the biogenic Rm-CuONPs obtained from Figure 1b

No. of peaks	Indices	Location (2θ)	FWHM (2θ)	Size (nm)	Strain (ε)
1	110	32.30	0.22611	52.21	0.22
2	−111	35.42	0.27247	50.26	0.26
3	111	38.92	0.29368	46.54	0.28
4	−202	48.65	0.34897	43.23	0.33
5	202	57.13	0.38719	42.46	0.36
6	113	61.59	0.43647	41.24	0.41
7	311	66.41	0.47198	38.84	0.45
8	202	68.23	0.48394	38.70	0.47
9	222	75.65	0.54328	28.39	0.51
			Average size	42.43	

determined by applying the equation ($\varepsilon = \beta \cos \theta/4$), and Table 1 includes a list of values.

The lattice parameters refer to the values that characterize a unit cell or the periodicity unit of the atomic arrangement. The lattice constants (parameters) of a unit cell comprise three dimensional lengths (a, b, and c) with their mutual angles (α, β, and γ). They have been explored using the X-ray diffraction (XRD) method and are regarded as most important structural aspects that potentially impact physical features [47]. The lattice parameters for the monoclinic RM-CuONPs structure were obtained by applying the following equation

$$a = \frac{\lambda}{\sqrt{3 \sin \theta \ 110}}$$

$$c = \frac{\lambda}{\sin\theta \ - 111}$$

The lattice parameters were computed, and the obtained results are presented in Table 2.

The functional moieties of the obtained by stabilized RM-CuONPs from RM-extract were detected FTIR by the spectral band identifications. The spectra of biosynthesized RM-CuONPs and RM extract are shown in Figure 3. Different functional peak stretches are observed at 3,440.52, 2,910.32, 2,852.14, 2,367.59, 1,614.80, 1,426.72, 1,065.08, 619.86, and 432.12 cm^{-1} for RM-CuONPs and at 3,442.86, 2,914.46, 2,856.75, 2,389.46, 1,620.72, 1,432.52, 1,094.46, 620.23, and 587.21 cm^{-1} for the RM-extract in the FTIR spectrum. Two broad absorption bands appeared in the higher energy region at 3,440.52 and 3,442.86 cm^{-1} in the FTIR spectra due to the –OH stretching of phenolic and flavonoid constituents [48]. The existence of absorption bands at 2,910.32 and 2,914.46 cm^{-1} is indicative of –C–H stretching (hydroxyl compound). The peaks at 2,852.14 and 2,856.75 cm^{-1} represent the H–C–H group. While the peaks that appeared at 2,367.59 and 2,389.46 cm^{-1} are allocated to stretching vibrations of C═O or N–H group [49]. The peak positions at 1614.80 and 1620.72 cm^{-1} were indicative of the existence of either the bending C═N vibration in the amide group or the stretching C═O vibration in the carboxyl group respectively [50]. The COO symmetric stretching corresponds to the observed bands at 1,426.72 and 1,432.52 cm^{-1} [51]. The appearance of sharp intensity bands at 1,065.08 and 1,094.46 cm^{-1} were indicative of C–O bond stretching (aromatic rings) [52], which can also be associated with the flavonoid and phenolic compounds found in the RE-extract. The bands observed at 619.86 and 620.23 cm^{-1} revealed the occurrence of C–H bending outside of the plane. However, the FTIR spectrum of RM-CuONPs exhibited two distinct intense bands at 522.12 and 432.12 cm^{-1} were attributed to Cu–O and Cu–N stretching vibrations, respectively, suggesting the strong interaction between NPs and plant biomolecules [53]. Moreover, a decrease in the intensities bands of functional group after reduction of Cu^{2+} ions suggests the involvement of phenol and flavonoid sites in binding RM-CuONPs [54]. The phenolic components present in the RM-extract assisted in the conversion of copper sulfate to CuO and stabilized the formation of RM-CuONPs. The occurrence of different types of phytocomponents (phenol, flavonoids, steroids, tannins, and carbohydrates) in the RM-extract facilitates the formation of RM-CuONPs by serving as reducing and capping agents. The obtained results collectively provide evidence for the successful reduction of CuO to CuONPs. Our findings were consistent with those of previously published studies, addressing the characterization of green-synthesized CuONPs [55].

The surface morphology and size of the pre-synthesized RM-CuONPs were studied using SEM and transmission electron microscopy (TEM) techniques. While EDX analysis was employed to examine the content of elements and distribution. The high-resolution SEM image clearly reveals that the resulting RM-CuONPs have a uniform distribution and rounded in shape with certain degree of agglomeration (Figure 4a). The existence of phytoconstituents in the RM-extract is most likely the cause of aggregation in RM-CuONPs,

Table 2: Values of lattice parameters of biogenic CuO

NP	2θ (110)	2θ (−111)	Lattice parameters	
			$a = b$	c
RM-CuONPs	32.30	35.42	3.2450	5.090

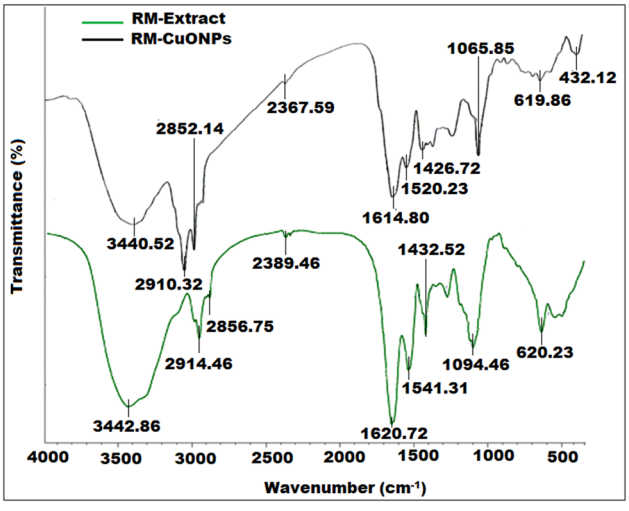

Figure 3: FTIR spectra of *R. microphylla* extract and biosynthesized RM-CuONPs.

due to the polarity and electrostatic interaction between the different particles of formed RM-CuONPs [56]. The nano size and spherical morphology of biosynthesized RM-CuONPs were further confirmed by the TEM visuals (Figure 4b), and the histogram for particle size distribution revealed a size range from 25.12 to 50.12 nm, with an average size of 32.45 nm (Figure 4c), which falls within the estimated range of the crystallite size found in the XRD analysis. A comparable size and shape of biosynthesized RM-CuONPs have been demonstrated in previous studies [57]. Furthermore, to get a deeper comprehension of the topographies of biogenic RM-CuONPs, the elemental composition and weight percentage of each element on the surface of formed NPs were estimated by EDX analysis. The elemental analysis validates the predominant presence of copper and oxygen in the formed nanostructure, indicating the high purity of the phyto-fabricated RM-CuONPs (Figure 4d). The weight and atomic percentage of copper (52.05 and 19.66%) and oxygen (32.42 and 49.02%) were determined, which and validated the formation of RM-CuONPs (Figure 4e). However, the appearance of a carbon signal in the EDX spectrum has been recognized as a consequence of residual organic plant extract contaminants (polyphenols, flavonoids, and proteins) on the NP or sample holder's surface coated in carbon tape. Moreover, the results of RM-CuONPs mapping also supported the findings of EDX spectrum (Figure 4f–g). Mapping results also showed that the biosynthesized NPs contain phytoconstituents that were in charge of biological activities.

3.2 Antimicrobial activity

The antimicrobial efficacy of RM-extract and RM-CuONPs was assessed against various microbes, including *S. epidermidis, E. faecalis, S. aureus, S. pneumoniae, B. subtilis, E. coli, E. cloacae, K. pneumoniae, P. aeruginosa, P. stuartii, S. typhi, C. albicans, and C. tropicalis*. Figure 5 illustrates the antibacterial effect of RM-extract and RM-CuONPs by a well diffusion assay against diverse bacteria. The results indicate that RM-CuONPs exhibit remarkable antimicrobial activity against all the tested strains compared to the RM-extract. The degree of microorganism susceptibility is reflected in the size of the inhibitory zone. Notably, Gram-positive strains were more sensitive to RM-CuONPs than Gram-negative pathogens as indicated in Table 3. Compared to Gram-positive pathogens; the resistance of the Gram-negative

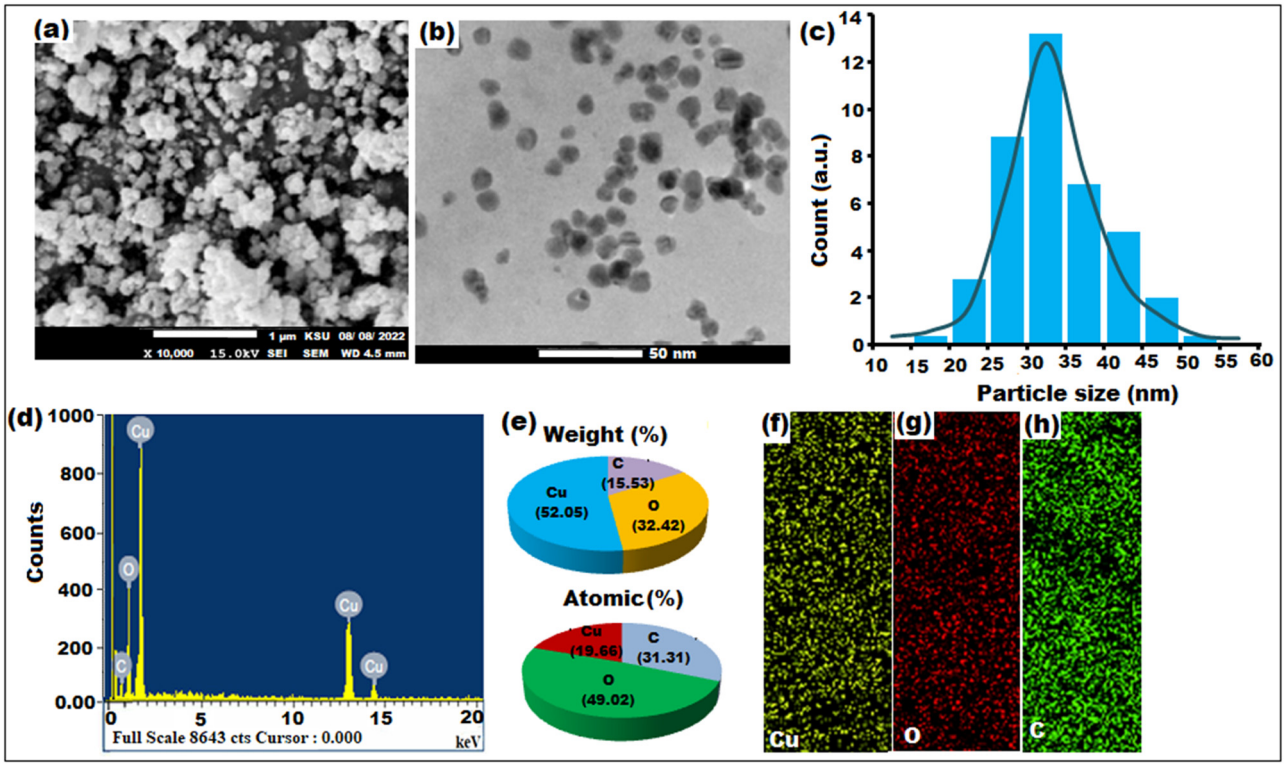

Figure 4: (a) SEM image, (b) TEM image, (c) particle size distribution histogram, (d) and (e) EDX spectrum, and (f)–(h) elemental mapping of biosynthesized RM-CuONPs from the RM extract.

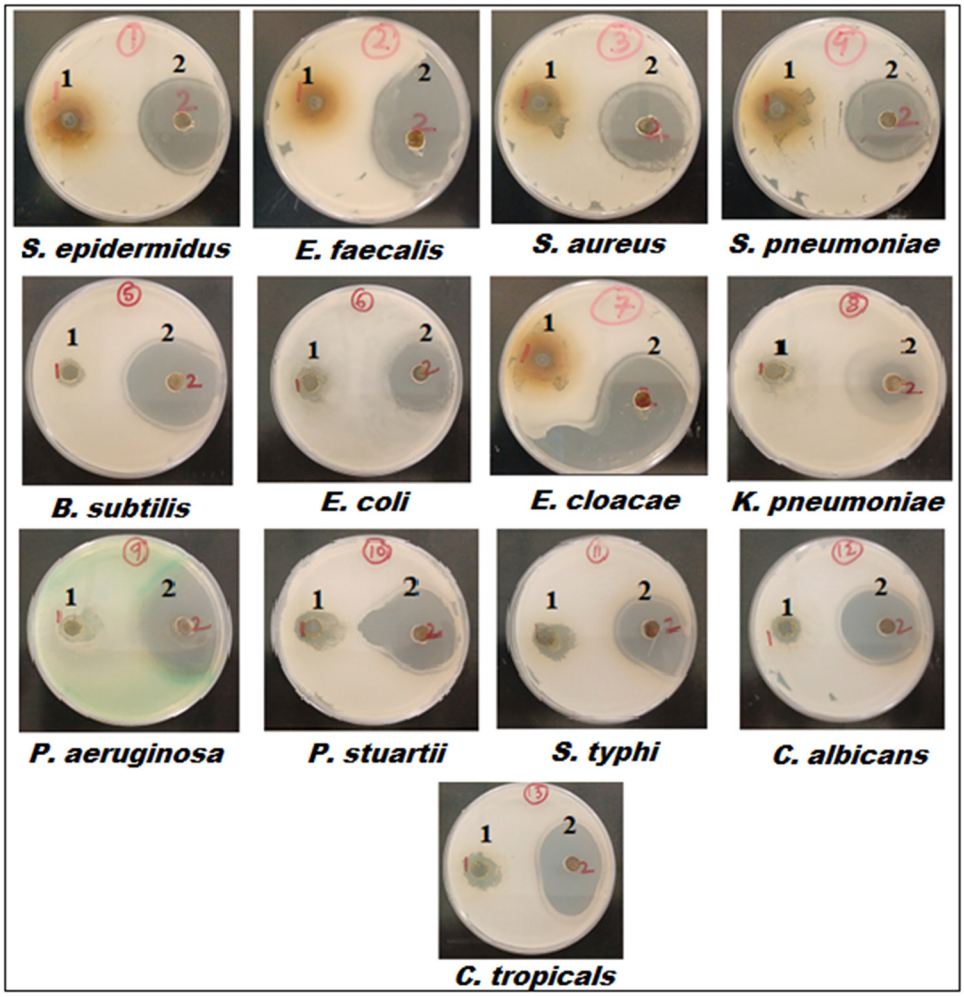

Figure 5: Well diffusion assay demonstrating the antibacterial activity of 1 – RM-extract and 2 – RM-CuONPs against 13 different microbial strains.

Table 3: Zone of Inhibition (mm) of RM-extract and biosynthesized RM-CuONPs

	Strains	Zone of inhibition	
		RM-extract	RM-CuONPs
Gram +ve	*S. epidermidis*	20 ± 1.5	45 ± 1.0
	E. faecalis	30 ± .1.2	40 ± 1.7
	S. aureus	18 ± 1	45 ± 1.5
	S. pneumoniae	20 ± 1.5	45 ± 2
	B. subtilis	20 ± 1.0	40 ± 1.0
Gram –ve	*E. coli*	15 ± 1.5	38 ± 1.0
	E. cloacae	20 ± 1.0	45 ± 00
	K. pneumoniae	15 ± 00	30 ± 1.0
	P. aeruginosa	20 ± 1.0	40 ± 00
	P. stuartii	25 ± 1.5	40 ± 1.0
	S. typhi	20 ± .00	35 ± 1.0
Fungi	*C. albicans*	20 ± 1.5	40 ± 1.00
	C. tropicalis	21 ± 1.00	45 ± 00

bacteria to the RM-CuONPs was higher. The distinct structure of Gram-negative bacteria's cell walls accounts for this variation. Gram-negative pathogens have an exterior coating of hydrophilic lipopolysaccharides that is considerably more resistant to the entry of antibacterial agents than the cell walls of Gram-positive bacteria. [37]. Furthermore, the degradation of antibiotic compounds is facilitated by the existence of enzymes in the periplasmic region of Gram-negative bacteria [58,59]. However, the fungal strains showed high sensitivity as compared to Gram-negative strains. As outlined in Table 3 and depicted in Figure 5, the RM-extract and RM-positive strains had inhibition zones measuring 20 ± 1.5 and 45 ± 1.0 mm, respectively, whereas best results among Gram-negative strains were shown towards *E. cloacae* with inhibition zones of 20 ± 1.0 and 45 ± 0.0 respectively. Similarly, RM-extract and RM-CuONPs exhibited the highest antifungal activity toward *C. tropicalis* with inhibition zones of 21 ± 10 mm and 45 ± 00 mm, respectively. Given that these three strains displayed the highest sensitivity to all tested

Table 4: Values of MIC and MBC for the RM-extract and biosynthesized RM-CuONPs

Strains	RM-extract		RM-CuONPs	
	MIC $mg \cdot mL^{-1}$	MBC $mg \cdot mL^{-1}$	MIC $\mu g \cdot mL^{-1}$	MBC $\mu g \cdot mL^{-1}$
S. epidermidis	3.15	12.5	48.5	97
E. cloacae	6.25	25	48.5	97
C. tropicalis	25	50	97	190

strains, they were exposed to MIC and MBC. Table 4 depicts the values of MIC and MBC for both the RM-extract and RM-CuONPs.

Even though the specific antimicrobial mechanism of metal oxide nanomaterials is still not fully understood, it is commonly believed that their antimicrobial effects result from several factors: direct interaction with bacterial cell membranes, generation of ROS, and free metal ions release from the nanomaterials [60,61]. The toxicity of copper and CuO toward various microorganisms operates through multiple concurrent mechanisms, ultimately leading to the demise of the microorganisms. The initial target site of copper-induced damage appears to be the microorganism's envelope [62]. The contact and breakdown of the pathogenic cell membrane, which permits the release of cytoplasmic components, is one of the hypothesized mechanisms underlying the antibacterial action [63]. The exposure of NPs can induce ROS generation, membrane permeability loss, cytoplasmic component leakage, and ultimately cell death [63]. The antibacterial action of CuNPs and CuONPs involves the destruction of cell membranes, ROS production, ribosomal instability, mitochondrial malfunction, lipid peroxidation, DNA degradation, and protein oxidation [64]. Copper ions inflict damage to nucleic acids following the copper binding specifically to DNA, and repeated cyclic redox reactions generate multiple hydroxyl radicals near the binding site, inflicting serious harm to nucleic acids (Figure 6). Nonetheless, it is plausible that, in certain pathogens, copper-induced oxidative disruption to genetic material could transpire via Fenton mechanism [65].

The effectiveness of RM-CuONPs in inhibiting the development of biofilm at sub-MIC doses was assessed towards *S. epidermidis*, *E. cloacae,* and *C. tropicalis*. As illustrated in Figure 7, the impact of RM-CuONPs on the biofilm formed by test strains demonstrated a concentration-dependent

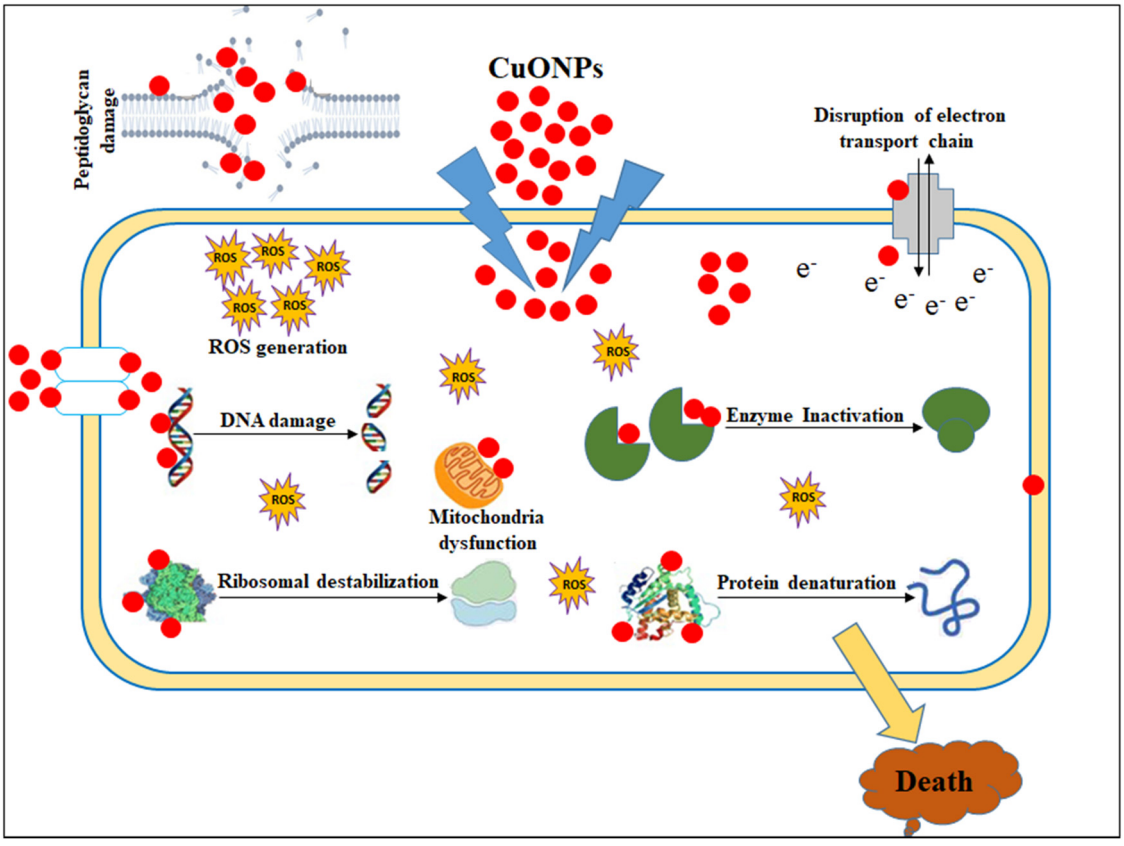

Figure 6: Schematic antibacterial mechanisms of CuONPs.

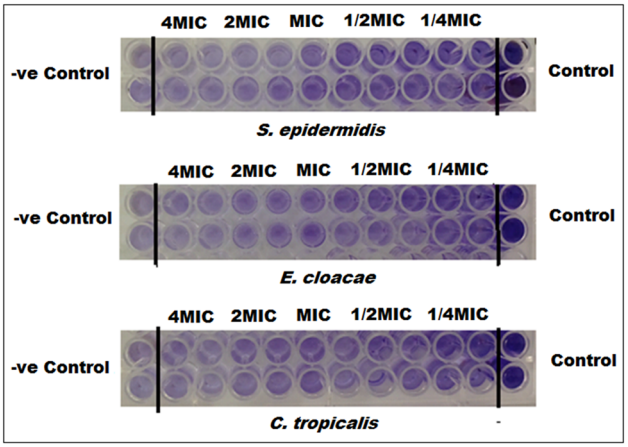

Figure 7: Microtiter plates demonstrating the anti-biofilm activity of RM-extract and RM-CuONPs.

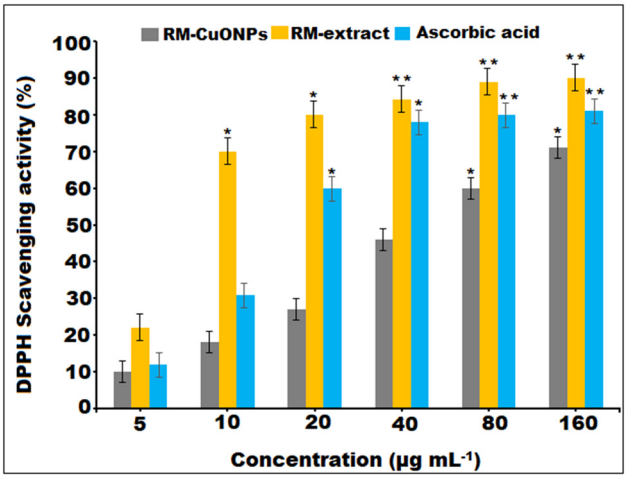

Figure 8: DPPH free radical scavenging activity of RM-CuONPs, RM-extract, and ascorbic acid at different concentrations.

inhibition. In the range from 4MIC to 2 MIC of RM-CuONPs, the biofilm was almost completely eradicated. However, biofilm eradication also declined as the concentration lowered further. At 1/2 MIC, and 1/4 MIC, the biofilm was not entirely eradicated (Figure 7). The study on the anti-biofilm activity of RM-CuONPs demonstrated an efficient reduction in biofilm formation by test strains. The increase in NP concentration corresponded to enhanced biofilm inhibition, indicating a dose-dependent activity. Within 3 days of exposure to RM-CuONPs, nearly all test strain biofilm cells were observed to perish. The bacterial biofilm poses a persistent global health threat due to its high resistance to treatment and its capacity to worsen infections [33]. Consequently, identifying effective compounds to address this challenge is of utmost importance. In this research, we evaluated the efficacy of RM-CuONPs against the biofilms formed by various microbes. This study represents a pioneering effort to assess the anti-biofilm properties of RM-CuONPs. The ability of antibacterial agents to hinder the development or breakdown of biofilms presents a hopeful avenue for minimizing microbial colonization on surfaces and epithelial mucosa.

The antimicrobial activity of results of biosynthesized RM-CuONPs was compared with previously reported green-synthesized CuONPs and demonstrated in Table 5. The findings clearly indicated that the biogenic RM-CuONPs have exerted strong antibacterial and antifungal potential compared to earlier studies.

3.3 Antioxidant activity

The antioxidant properly of RM-CuONPs, aqueous RM-extract, and standard L-ascorbic acid is depicted in Figure 8. The obtained results showed that the DPPH scavenging potential of RM-CuONPs, aqueous RM-extract, and L-ascorbic acid at six varied doses (5–140 µg·mL^{-1}) with the ranges being 10.68 to 76.12%, 24.02 to 87.90%, and 15.68 to 82.02%, respectively.

Table 5: Antibacterial properties of green-synthesized CuONPs using different plant extracts

Plant name	Part used	NP	Antimicrobial activity	MIC/MBC (µg·mL^{-1})	Reference
Mangifera Indica	Leaves	CuONPs	Antibacterial	120	[66]
Aegle marmelos	Leaves	CuONPs	Antibacterial	125	[67]
Terminalia chebula	Fruits	CuONPs	Antibacterial	250	[68]
Olea europaea	Leaves	CuONPs	Antibacterial	250	[69]
Balanites aegyptiaca	Stem bark	CuONPs	Antibacterial	100	[70]
Aerva javanica	Leaves	CuONPs	Antibacterial, antifungal	128, 160	[39]
Cedrus deodara	Leaves	CuONPs	Antibacterial	25	[71]
Catha edulis	Leaves	CuONPs	Antibacterial	250	[72]
Ailanthus altissima	Leaves	CuONPs	Antibacterial	20	[73]
Eupatorium odoratum	Leaves	CuONPs	Antibacterial	100	[74]
Acanthospermum hispidum	Leaves	CuONPs	Antibacterial	100	[74]

The scavenging effect caused by RM-CuONPs was demonstrated by the DPPH assay findings, which showed an IC50 value of 29.12 ± 0.02 μg mL^{-1} for RM-CuONPs in comparison to 6.48 ± 0.01 μg mL^{-1} for RM-extract and 12.25 ± 0.04 μg mL^{-1} for reference ascorbic acid. Additionally, it was found that the RM-extract had enhanced potential for antioxidants than the reference L-ascorbic acid and RM-CuONPs, which might be due to occurrence of various bioactive components with increased phenolics and flavonoids content in the aqueous extract of RM plant.

4 Conclusions

The current research demonstrated the characterization, antimicrobial activity, anti-biofilm effect, and antioxidant prospective of green synthesized RM-CuONPs using an aqueous extract of RM. The characteristic features and quality of biogenic RM-CuONPs were examined by several sophisticated analytical techniques. The results of the investigation revealed that the RM plant extract efficiently reduced and stabilized the produced NPs. The outcome of the bio-fabricated approach yielded spherical and monoclinical structured RM-CuONPs with an average size of 32.45 nm. The FTIR analysis corroborated the formation of NPs with the appearance of broad absorption bands at 522.12 and 432.12 cm^{-1} for the RM-CuONPs. The formed biogenic RM-CuONPs showed remarkable antibacterial potential toward a panel of bacteria. RM-CuONPs exhibited considerable dose-dependent antibiofilm effects against *S. epidermidis, E. cloacae,* and *C. tropicalis.* These findings suggest that RM-CuONPs hold promise as effective antibiofilm agents against pathogenic microorganisms. Nonetheless, further investigation is required to ascertain their clinical efficacy and toxicity profile before considering clinical applications. Moreover, the biosynthesized RM-CuONPs have been observed to possess antioxidant potential with an IC_{50} value of 29.12 ± 0.02 μg·mL^{-1} toward the DPPH assay. In conclusion, the findings of this investigation validate the significance of RM-CuONPs mediated by RM extract as potential biological agents. These nanostructures offer a promising substitute for conventional medications in combating multi-drug-resistant pathogens. However, further studies are required to establish the biochemical processes and accountable mechanisms for the antibacterial and antioxidant activities.

Acknowledgements: This work was funded by the Researchers Supporting Project number (RSP2024R294), King Saud University, Riyadh, Saudi Arabia.

Funding information: This research was funded by the Researchers Supporting Project number (RSP2024R294), King Saud University, Riyadh, Saudi Arabia.

Author contributions: N.M.A.M.: conceptualization M.A. and H.M.A-Y.: formal analysis, M.H.: validation and figures, R.S.B.: biology methodology, writing – review and editing, visualization, data curation, S.A-D.: writing – review and editing. All authors have read and agreed to the published version of the manuscript.

Conflict of interest: The authors state no conflict of interest.

Data availability statement: All data generated or analyzed during this study are included in this published article.

References

[1] Alshammari BH, Lashin MM, Mahmood MA, Al-Mubaddel FS, Ilyas N, Rahman N, et al. Organic and inorganic nanomaterials: fabrication, properties and applications. RSC Adv. 2023;13(20):13735–85.
[2] Sun LG, Wu G, Wang Q, Lu J. Nanostructural metallic materials: Structures and mechanical properties. Mater Today. 2020;38(31):114–35.
[3] Nikolova MP, Chavali MS. Metal oxide nanoparticles as biomedical materials. Biomimetics. 2020;5(2):27.
[4] Cuong HN, Pansambal S, Ghotekar S, Oza R, Hai NT, Viet NM, et al. New frontiers in the plant extract mediated biosynthesis of copper oxide (CuO) nanoparticles and their potential applications: A review. Env Res. 2022;203:111858.
[5] Rabiee N, Bagherzadeh M, Kiani M, Ghadiri AM, Etessamifar F, Jaberizadeh AH, et al. Biosynthesis of copper ox-ide nanoparticles with potential biomedical applications. Int J Nanomed. 2020;2020(15):3983–99.
[6] Muthuvel A, Jothibas M, Manoharan C. Synthesis of copper oxide nanoparticles by chemical and biogenic methods: photocatalytic degradation and in vitro antioxidant activity. Nanotechnol Environ Eng. 2020;5(2):14–9.
[7] Menazea AA, Ahmed MK. Silver and copper oxide nanoparticles-decorated graphene oxide via pulsed laser ablation technique: Preparation, characterization, and photoactivated antibacterial activity. Nano-Struct Nano-Objectss. 2020;22:100464.
[8] Luna IZ, Hilary LN, Chowdhury AS, Gafur MA, Khan N, Khan RA. Preparation and characterization of copper oxide nanoparticles synthesized via chemical precipitation method. OALibJ. 2015;2(3):1–8.
[9] Keabadile OP, Aremu AO, Elugoke SE, Fayemi OE. Green and traditional synthesis of copper oxide nanoparti-cles—comparative study. Nanomater. 2020;10(12):2502.
[10] Waris A, Din M, Ali A, Ali M, Afridi S, Baset A, et al. A comprehensive review of green synthesis of copper oxide nanoparticles and their

diverse biomedical applications. Inorg Chem Commun. 2021;123:108369.
[11] Letchumanan D, Sok SP, Ibrahim S, Nagoor NH, Arshad NM. Plant-based biosynthesis of copper/copper oxide nano-particles: an update on their applications in biomedicine, mechanisms, and toxicity. Biomolecules. 2021;11(4):564.
[12] Eltaweil AS, Fawzy M, Hosny M, Abd El-Monaem EM, Tamer TM, Omer AM. Green synthesis of platinum nanoparticles using *Atriplex halimus* leaves for potential antimicrobial, antioxidant, and catalytic applications. Arab J Chem. 2022;15(1):103517.
[13] Bordiwala RV. Green synthesis and applications of metal nano-particles.-A review article. Results Chem. 2023;5:100832.
[14] Yi T, Miller AJ, Wen J. Phylogenetic and biogeographic diversification of *Rhus* (Anacardiaceae) in the Northern Hemi-sphere. Mol Phylogenet Evol. 2004;33(3):861–79.
[15] Charles-Rodríguez AV, Rivera-Solis LL, Martins JT, Genisheva Z, Robledo-Olivo A, Gonzalez-Morales S, et al. Edible films based on black chia (*Salvia hispanica* L.) seed mucilage containing *Rhus microphylla* fruit phenolic extract. Coat. 2020;10(4):326.
[16] Martinez EM, Sandate-Flores L, Rodriguez-Rodríguez J, Rostro-Alanis M, Parra-Arroyo L, Antunes-Ricardo M, et al. Underutilized Mexican plants: Screening of antioxidant and antiproliferative properties of Mexican cactus fruit juices. Plants. 2021;10(2):368.
[17] Guia-Garcia JL, Charles-Rodriguez AV, Lopez-Romero JC, Torres-Moreno H, Genisheva Z, Robledo-Olivo A, et al. Phenolic composition and biological prop-erties of *Rhus microphylla* and *Myrtillocactus geometrizans* fruit extracts. Plants. 2021;10(10):2010.
[18] Flores-Lopez ML, Guia-Garcia JL, Lopez-Romero JC, Torres-Moreno H, Moo-Huchin VM, Garcia-Munguia AM, et al. *Rhus microphylla* leaves extracts obtained by ohmic heating: Physicochemical composition and bioactive properties. Ind Crop Prod. 2024;213:118417.
[19] Jamal M, Mondal S, Ayon SA, Mim SR, Islam MS, Billah MM. Phase engineered enhancement of multifaceted properties of cuo nanoparticles: a fluorine and gadolinium doping approach. Available at SSRN 4732183.
[20] Liu Y, Shi L, Su L, van der Mei HC, Jutte PC, Ren Y, et al. Nanotechnology-based antimicrobials and delivery systems for biofilm-infection control. Chem Soc Rev. 2019;48(2):428–46.
[21] Elbourne A, Truong VK, Cheeseman S, Rajapaksha P, Gangadoo S, Chapman J, et al. The use of nanomaterials for the mitigation of pathogenic biofilm formation. Methods Microbiol. Academic Press 2019;46:61–92.
[22] Pang H, Gao F, Lu Q. Morphology effect on antibacterial activity of cuprous oxide. Chem Comm. 2009;9:1076–8.
[23] McDonnell G, Russell AD. Antiseptics and disinfectants: activity, action, and resistance. Clin Microbiol Rev. 1999;12(1):147–79.
[24] Ren G, Hu D, Cheng EW, Vargas-Reus MA, Reip P, Allaker RP. Characterisation of copper oxide nanoparticles for antimicrobial applications. Int J Antimicrob Agents. 2009;33(6):587–90.
[25] Montero DA, Arellano C, Pardo M, Vera R, Galvez R, Cifuentes M, et al. Antimicrobial properties of a novel copper-based composite coating with potential for use in healthcare facilities. Antimicrob Resist Infect Control. 2019;8(3):1–10.
[26] Ma X, Zhou S, Xu X, Du Q. Copper-containing nanoparticles: Mechanism of antimicrobial effect and application in dentistry-a narrative review. Front surg. 2022;9:905892.
[27] Alali A, Hosseini-Abari A, Bahrami A, Yazdan MM. Biosynthesis of copper oxide and silver nanoparticles by *bacillus* spores and evaluation of the feasibility of their use in antimicrobial paints. Mater. 2023;16(13):4670.
[28] Vimbela GV, Ngo SM, Fraze C, Yang L, Stout DA. Antibacterial properties and toxicity from metallic nanomaterials. Int J Nanomed. 2017;12:3941–65.
[29] Slavin YN, Asnis J, Hńfeli UO, Bach H. Metal nanoparticles: understanding the mechanisms behind antibacterial activity. J Nanobiotechnol. 2017;15(65):1–20.
[30] Ermini ML, Voliani V. Antimicrobial nano-agents: the copper age. ACS Nano. 2021;15(4):6008–29.
[31] Singh J, Dutta T, Kim KH, Rawat M, Samddar P, Kumar P. Green'synthesis of metals and their oxide nanoparticles: applications for environmental remediation. J Nanobiotechnol. 2018;16(84):1–24.
[32] Mirghani R, Saba T, Khaliq H, Mitchell J, Do L, Chambi L, et al. Biofilms: Formation, drug resistance and alternatives to conventional approaches. AIMS Microbiol. 2022;8(3):239–77.
[33] Khan J, Tarar SM, Gul I, Nawaz U, Arshad M. Challenges of antibiotic resistance biofilms and potential combating strategies: a review. 3 Biotech. 2021;11(4):169.
[34] Bhat RS, Al-Daihan S, Al-Dbass AM. Anti-biofilm and antimicrobial activity of sodium fluoride against various pathogenic microbes. Fluoride. 2024;5(1):1.
[35] Khatoon Z, McTiernan CD, Suuronen EJ, Mah TF, Alarcon EI. Bacterial biofilm formation on implantable devices and approaches to its treatment and prevention. Heliyon. 2018;4(12):e01067.
[36] Nobile CJ, Johnson AD. *Candida albicans* biofilms and human disease. Annu Rev Microbiol. 2015;69:71–92.
[37] Breijyeh Z, Jubeh B, Karaman R. Resistance of gram-negative bacteria to current antibacterial agents and approaches to resolve it. Molecules. 2020;25(6):1340.
[38] Bezza FA, Tichapondwa SM, Chirwa EM. Fabrication of monodispersed copper oxide nanoparticles with potential application as antimicrobial agents. Sci Rep. 2020;10(1):16680.
[39] Amin F, Khattak B, Alotaibi A, Qasim M, Ahmad I, Ullah R, et al. Green synthesis of copper oxide nanoparticles using *Aerva javanica* leaf extract and their characterization and investigation of in vitro antimicrobial potential and cytotoxic activities. Evid Based Complementary Altern Med. 2021;2021:5589703.
[40] Letchumanan D, Sok SP, Ibrahim S, Nagoor NH, Arshad NM. Plant-based biosynthesis of copper/copper oxide nanoparticles: an update on their applications in biomedicine, mechanisms, and toxicity. Biomolecules. 2021;11(4):564.
[41] Schlesier K, Harwat M, Böhm V, Bitsch R. Assessment of antioxidant activity by using different in vitro methods. Free Radic Res. 2002;36(2):177–87.
[42] Kulkarni D, Sherkar R, Shirsathe C, Sonwane R, Varpe N, Shelke S, et al. Biofabrication of nanoparticles: sources, synthesis, and biomedical applications. Front Bioeng Biotechnol. 2023;11:1159193.
[43] Yugandhar P, Vasavi T, Uma Maheswari Devi P, Savithramma N. Bioinspired green synthesis of copper oxide nanoparticles from *Syzygium alternifolium* (Wt.) Walp: characterization and evaluation of its synergistic antimicrobial and anticancer activity. Appl Nanosci. 2017;7:417–27.
[44] Sagadevan S, Pal K, Chowdhury ZZ. Fabrication of CuO nanoparticles for structural, optical and dielectric analysis using chemical precipitation method. J Mater Sci: Mater Electron. 2017;28:12591–7.
[45] Thakar MA, Jha SS, Phasinam K, Manne R, Qureshi Y, Babu VH. X ray diffraction (XRD) analysis and evaluation of antioxidant activity of copper oxide nanoparticles synthesized from leaf extract of *Cissus vitiginea*. Mater Today Proc. 2022;51(Part1):319–24.

[46] Taghavi FS, Moradnia F, Heidarzadeh S, Naghipour A. Green synthesis, characterization, photocatalytic and antibacterial activities of copper oxide nanoparticles of copper oxide nanoparticles. Nanochem Res. 2023;8(2):134–40.
[47] Lakshmanan SP, Jostar ST, Arputhavalli GJ, Jebasingh S, Josephine CM. Role of Green Synthesized CuO Nanoparticles of *Trigonella Foenum*- Graecum L. Leaves and their Impact on Structural, Optical and Antimicrobial Activity. Int J Nanosci. 2021;17(2):109–21.
[48] Wongsa P, Phatikulrungsun P, Prathumthong S. FT-IR characteristics, phenolic profiles and inhibitory potential against digestive enzymes of 25 herbal infusions. Sci Rep. 2022;12(1):6631.
[49] Bhat RS, Alghamdi JM, Aldbass AM, Aljebrin NA, Alangery AB, Soliman DA, et al. Biochemical and FT-IR profiling of *Tritium aestivum* L. seedling in response to sodium fluoride treatment. Fluoride. 2022;55(1):81–9.
[50] Ganaie TA, Masoodi FA, Rather SA, Wani SM. Physicochemical, antioxidant and FTIR-ATR spectroscopy evaluation of Kashmiri honeys as food quality traceability and Himalayan brand. J Food Sci Technol. 2021;58(11):4139–48.
[51] Bhat RS, Al-Dbass AM, Alghamdia JM, Alonazia MA, Al-Daihan S. *Trigonella foenum-graecum* l. Seed germination under sodium halide salts exposure. Fluoride. 2023;56(2):169–79.
[52] Arik KEA, Us F. Evaluation of structural properties of cellulose ether-corn starch based biodegradable films. Int J Polym Mater Polym Biomater. 2014;63(7):342–51.
[53] Kalaiyarasi M, Nivedha M, Mani M, Harikrishnan R, Kumar JK, Loganathan S, et al. Synthesis of CuO/NaCuSO4 nanocomposite using an aqueous extract of *TribulusTerrestris* and their structural, optical, morphology and dielectric studies. Chem Pap. 2024;78:3083–98.
[54] Soni A, Kaushal D, Kumar M, Sharma A, Maurya IK, Kumar S. Synthesis, characterizations and antifungal activities of copper oxide and differentially doped copper oxide nanostructures. Mater Today Proc. 2022 Sep 22.
[55] Bhat AA, Thoker BA, Wani AK, Sheergojri GA, Kaloo MA, Bhatd BA, et al. Synthesis and characterization of copper oxide nanoparticles by co-precipitation method: electronic and antimicrobial properties. Chem Sci Eng Res. 2021;3(6):25–9.
[56] Ahmadian Y, Bakravi A, Hashemi H, Namazi H. Synthesis of polyvinyl alcohol/CuO nanocomposite hydrogel and its application as drug delivery agent. Polym Bull. 2019;76:1967–83.
[57] Dey A, Manna S, Chattopadhyay S, Mondal D, Chattopadhyay D, Raj A, et al. *Azadirachta indica* leaves mediated green synthesized copper oxide nanoparticles induce apoptosis through activation of TNF-α and caspases signaling pathway against cancer cells. J Saudi Chem Soc. 2019;23(2):222–38.
[58] Miller SI, Salama NR. The gram-negative bacterial periplasm: Size matters. PLoS Biol. 2018;16(1):e2004935.
[59] Munita JM, Arias CA. Mechanisms of antibiotic resistance.Virulence mechanisms of bacterial pathogens. Microbiol Spectr. 2016;4(2):481–511.
[60] Chan YB, Aminuzzaman M, Rahman MK, Win YF, Sultana S, Cheah SY, et al. Green synthesis of ZnO nanoparticles using the mangosteen (*Garcinia mangostana* L.) leaf extract: Comparative preliminary in vitro antibacterial study. Green Process Synth. 2024;13(1):20230251.
[61] Tan EP, Djearamane S, Wong LS, Rajamani R, Tanislaus Antony AC, Subbaih SK, et al. An in vitro study of the antifungal efficacy of zinc oxide nanoparticles against Saccharomyces cerevisiae. Coatings. 2022;12(12):1988.
[62] Mathews S, Hans M, Mücklich F, Solioz M. Contact killing of bacteria on copper is suppressed if bacterial-metal contact is prevented and is induced on iron by copper ions. Appl Environ Microbiol. 2013;79(8):2605–11.
[63] Sharma P, Goyal D, Chudasama B. Antibacterial activity of colloidal copper nanoparticles against Gram-negative (Escherichia coli and Proteus vulgaris) bacteria. Lett Appl Microbiol. 2022;74(5):695–706.
[64] Chatterjee AK, Chakraborty R, Basu T. Mechanism of antibacterial activity of copper nanoparticles. Nanotechnol. 2014;25(13):135101.
[65] Warnes SL, Keevil CW. Mechanism of copper surface toxicity in vancomycin-resistant enterococci following wet or dry surface contact. Appl Environ Microbiol. 2011;77(17):6049–59.
[66] Dat NM, Nam NT, An H, Cong CQ, Hai ND, Phong MT, et al. Green synthesis of copper oxide nanoparticles for photodegradation of malachite green and antibacterial properties under visible light. Opt Mater. 2023;136:113489.
[67] Ali SG, Haseen U, Jalal M, Khan RA, Alsalme A, Ahmad H, et al. Green synthesis of copper oxide nanoparticles from the leaves of *Aegle marmelos* and their antimicrobial activity and photocatalytic activities. Molecules. 2023;28(22):7499.
[68] Munusamy T, Shanmugam R. Green synthesis of copper oxide nanoparticles synthesized by *Terminalia chebula* dried fruit extract: characterization and antibacterial action. Cureus. 2023;15(12):e50142.
[69] Binjawhar DN, Alsharari SS, Albalawi A, Abdulhasan MJ, Khat M, Ameen F. Facile green synthesis inorganic cuprous oxide nanoparticles and their antibacterial properties. Micro Nano Lett. 2023;18(1):e12154.
[70] Teklu B, Kadiri SK, Vidavalur S. Green synthesis of copper oxide nanoparticles using Balanites aegyptiaca stem bark extract and investigation of antibacterial activity. Results Chem. 2023;6:101152.
[71] Ramzan M, Obodo RM, Mukhtar S, Ilyas SZ, Aziz F, Thovhogi N. Green synthesis of copper oxide nanoparticles using Cedrus deodara aqueous extract for antibacterial activity. Mater Today: Proc. 2021;36:576–81.
[72] Andualem WW, Sabir FK, Mohammed ET, Belay HH, Gonfa BA. Synthesis of copper oxide nanoparticles using plant leaf extract of Catha edulis and its antibacterial activity. J Nanotechnol. 2020;2020(1):2932434.
[73] Awwad A, Amer M. Biosynthesis of copper oxide nanoparticles using Ailanthus altissima leaf extract and antibacterial activity. Chem Inter. 2020;6(4):210–17.
[74] Gowri M, Latha N, Rajan M. Copper oxide nanoparticles synthesized using Eupatorium odoratum, *Acanthospermum hispidum* leaf extracts, and its antibacterial effects against pathogens: a comparative study. BioNanoScience. 2019;9:545–52.